210/211, 577 (1992).
13. D. K. Schwartz, J. Garnaes, R. Viswanathan, J. A. N. Zasadzinski, *Science* **257**, 508 (1992); D. K. Schwartz, J. Garnaes, R. Viswanathan, S. Chiruvolu, J. A. N. Zasadzinski, *Phys. Rev. E* **47**, 452 (1993).
14. J. Garnaes, D. K. Schwartz, R. Viswanathan, J. A. N. Zasadzinski, *Nature* **357**, 54 (1992).
15. Arachidic or palmitic acid (Sigma, >99%) LB multilayers were transferred to mica or thermally oxidized silicon substrates by the conventional vertical deposition method from a 0.5 mM $CdCl_2$ subphase (Millipore water was used), adjusted to pH = 6.5, and contained in a Nima (Coventry, England) LB trough. Imaging was performed with the use of a Nanoscope III Multimode atomic force microscope (Digital Instruments) in contact mode using a silicon nitride cantilever with integral tip. The equilibrium deflection of a given cantilever was quite sensitive to temperature; therefore, the tip was withdrawn before large temperature jumps and re-engaged after the temperature had stabilized. A small thermoelectric Peltier element (Melcor, Trenton, NJ) and a thermocouple (Omega Engineering, Stanford, CT) were sandwiched between a magnetic stainless steel base and a small piece of copper sheet and bonded together with thermally conductive epoxy. The entire assembly was less than 5 mm thick and 12 mm in cross section. Extremely thin and flexible electrical leads were carefully strain-relieved to avoid transmission of vibrations to the microscope. Over the usable temperature range of the device, 20° to 120°C, the scanner temperature remained below 35°C, minimizing difficulties associated with thermal drift. A previously reported temperature-controlled microstage (*16*) functioned only below 80°C. Several important control experiments were performed to validate the technique. Invariant molecular-resolution images of mica substrates were obtained to well above 100°C. High-resolution images of all three types of structure were quantitatively consistent after changing the scan size or rate, rotating the scan direction, or annealing at constant temperature for hours. The surface structure changed at the same temperature in nine separate repetitions of the experiment (using different samples and AFM tips) and reversibly changed back upon lowering of the temperature while using the same tip. On one occasion, we were even able to maintain the tip in contact with the film during this thermal cycling and continuously observed the loss and then reappearance of molecular order. These experiments prove that the loss of molecular resolution was due to increased molecular disorder, not degradation of a particular tip, and that the images represent structure indigenous to the sample, not related to temporal noise or induced by scanning.
16. I. Musevic, G. Slak, R. Blinc, *Rev. Sci. Instrum.* **67**, 2554 (1996).
17. J. Toner and D. R. Nelson, *Phys. Rev. B* **23**, 316 (1981).
18. J. Y. Josefowicz *et al.*, *Science* **260**, 323 (1993).
19. D. G. Cameron and R. A. Dluhy, in *Spectroscopy in the Biomedical Sciences*, R. M. Gendreau, Ed. (CRC Press, Boca Raton, FL, 1986), pp. 53–86.
20. Transmission IR spectra were recorded with the use of a Mattson Cygnus 100 spectrometer with a 6.4-mm pinhole defining the incident beam. The sample holder was heated using a thin film resistive heating element (Minco, Minneapolis, MN); the temperature was measured with a thermocouple (Omega). After obtaining the multilayer spectrum, the sample holder was removed and placed in an ultraviolet-oxygen cleaner (Boekel Industries, Feasterville, PA), where the film on both sides of the substrate was removed. The holder was then repositioned within the spectrometer, to within 0.1 mm of the original position, and the background spectrum was measured.
21. C.-Y. Chao, C.-F. Chou, J. T. Ho, A. Jin, C. C. Huang, *Phys. Rev. Lett.* **77**, 2750 (1996).
22. We thank D. R. Nelson for his helpful comments regarding 2D melting. This work was supported by the National Science Foundation (NSF), the donors of the Petroleum Research Fund, and the Center for Photoinduced Processes (funded by NSF and the Louisiana Board of Regents).

5 May 1997; accepted 17 October 1997

Enhanced Intergrain Tunneling Magnetoresistance in Half-Metallic CrO_2 Films

H. Y. Hwang and S.-W. Cheong

Low-field tunneling magnetoresistance was observed in films of half-metallic CrO_2 that were grown by high-pressure thermal decomposition of CrO_3. High-temperature annealing treatments modified the intergrain barriers of the as-grown films through surface decomposition of CrO_2 into insulating Cr_2O_3, which led to a threefold enhancement of the low-field magnetoresistance. This enhancement indicates the potential of this simple method to directly control the interface barrier characteristics that determine the magnetotransport properties.

Half-metallic ferromagnets exhibit conducting states at the Fermi level (E_F) for majority-spin electrons, but a semiconductor gap for minority-spin electrons (*1*). The resulting high degree of spin-polarization of Fermi-level electrons suggests that this class of materials could exhibit enhanced spin-dependent magnetotransport. Transition metal oxides can exhibit half-metallic behavior, in part because of their narrow conduction bands derived from transition metal *d* levels and oxygen *p* levels. Recently, low-field spin-polarized tunneling magnetoresistance (MR) was observed in polycrystalline perovskite manganites, layered manganites, artificial thin-film trilayer structures of perovskite manganites, and polycrystalline pyrochlore $Tl_2Mn_2O_7$, all of which are (or are suspected to be) half-metallic ferromagnets (*2–6*). In another example, perovskite manganite electrodes were used to inject spin-polarized carriers into a high-temperature superconductor, which suppressed the critical current by pair breaking (*7*).

All of the oxide systems currently investigated for tunneling MR are Mn-based, although this phenomenon should not be specific to the manganites. Half-metallic ferromagnetism has been suspected in the technologically important CrO_2. Already a staple magnetic recording medium, band structure calculations of CrO_2 predict 100% spin polarization at E_F (*8*). Spin-polarized photoemission and vacuum tunneling experiments show nearly complete spin polarization 2 eV below E_F, but a negligible density of states at E_F, inconsistent with metallic behavior (*9*, *10*). Because CrO_2 has a higher Curie temperature (T_C = 395 K) than all of the aforementioned systems and is already processed in large volumes in industry, it is a promising material in which to explore tunneling MR.

Previous studies of single-crystal CrO_2 report little MR below T_C, but in analogy to a recent comparison of single crystal and polycrystalline perovskite manganites, polycrystalline CrO_2 might exhibit low-field intergrain tunneling MR (*3*). We studied polycrystalline CrO_2 films grown by high-pressure thermal decomposition of CrO_3 on $SrTiO_3$ substrates and observed significant low-field spin-polarized tunneling MR at low temperatures in as-grown films. High-temperature annealing treatments significantly enhance low-field MR by modification of the effective intergrain tunneling barrier through surface decomposition of CrO_2 into insulating Cr_2O_3. This method provides a convenient way to control the interface properties for tunneling MR.

We prepared polycrystalline films of CrO_2 by dissolving CrO_3 powders in deionized water. The solution was uniformly applied on single-crystal $SrTiO_3$ substrates. Curing the specimen in a dry-air atmosphere removed the water and left a thin layer (typically a few micrometers) of polycrystalline CrO_3. Treatment in a few hundred bars of oxygen pressure with increasing temperature led to a series of decomposition reactions $CrO_3 \rightarrow (Cr_3O_8 \rightarrow Cr_2O_5) \rightarrow CrO_2 \rightarrow Cr_2O_3$, which are very sensitive to the applied temperature and pressure (*11*). Furthermore, only under high oxygen pressure does a narrow but distinct temperature window exist for stable, single-phase CrO_2. Because CrO_2 is metallic whereas CrO_3 and Cr_2O_3 are insulating, monitor-

H. Y. Hwang, Bell Laboratories, Lucent Technologies, Murray Hill, NJ 07974, USA.
S.-W. Cheong, Bell Laboratories, Lucent Technologies, Murray Hill, NJ 07974, and Department of Physics and Astronomy, Rutgers University, Piscataway, NJ 08855, USA.

ing the resistivity during the decomposition process and subsequent annealing allows precise control of the sample growth. Gold electrode pads evaporated directly on the $SrTiO_3$ substrate and gold wire leads were used for standard four-probe resistivity measurements throughout the high-temperature, high-pressure treatment.

The morphology of the resulting films was studied by scanning electron microscopy (SEM). The grains were generally elongated shapes, ~2 μm in the long dimension. The distribution of grain sizes was fairly broad, however. The large-scale structure of the grains appears to be predetermined by the preparation of the CrO_3 film, as the thermal decomposition reaction to CrO_2 occurs at fairly low temperature (~450°C). Thus, the detailed methodology of CrO_3 decomposition can likely vary the CrO_2 grain size and shape.

Previous reports of the temperature-dependent resistivity [$\rho(T)$] of CrO_2 vary widely, from semiconducting to metallic, and range over five orders of magnitude at low temperatures (Fig. 1) (*12–14*). Whereas bulk and film single crystals all exhibit good metallic behavior, particularly the polycrystalline samples seem quite variable. In two of our polycrystalline films upon heating (during growth) and cooling to low temperature, the formation of CrO_2 corresponds to the sharp decrease in ρ at 722 K at 200-bar oxygen pressure (Fig. 1). At this point the sample can be cooled, and stable, single-phase CrO_2 film remains (film II). However, further heating leads to the partial reduction of CrO_2 to Cr_2O_3, an insulator. Approaching this second phase boundary, ρ began to increase rapidly. In film I, ρ was allowed to increase before quenching to room temperature. Although at low temperatures ρ is more than three orders of magnitude greater, the magnetization (M) still reflects ferromagnetic CrO_2 (Fig. 2). In both cases, we observe magnetic properties consistent with high-quality bulk CrO_2. Heating the films in various atmospheres (or vacuum) did not affect the films below 150°C.

Insight into the process raising ρ in film I can be obtained by comparing the x-ray diffraction pattern of the two films (Fig. 3). The films were measured by means of a powder x-ray diffractometer with Co K_α radiation. The first observation was to confirm the randomly oriented polycrystalline nature of the films. In both films, peaks corresponding to the polycrystalline pattern of CrO_2 tetragonal rutile structure are observed. The higher resistive film (film I) displays weak but distinct rhombohedral Cr_2O_3 peaks that are absent in the other film, even though the highest annealing temperature was kept below the bulk thermodynamic phase boundary. The magnetic properties were completely unchanged in the second film, aside from possible corrections due to the presence of antiferromagnetic Cr_2O_3. This result indicates that with high-temperature annealing, the CrO_2 grains are not uniformly degrading (usually the magnetic properties such as the coercive field are highly sensitive to crystallinity).

We have studied a number of samples with intermediate ρ values between the two films discussed here. Films that exhibit increases in ρ in this range do not show clear Cr_2O_3 peaks, but are likely systematically varying in the expected manner. These results indicate that with the initial increase in ρ, the surface of the CrO_2 grains reduces into Cr_2O_3, whereas the interior of the grains remains unaffected. With increasing ρ, the films begin to have a greenish hue, the color of Cr_2O_3. This tendency toward surface degradation has been observed in photoemission studies where the spectrum displayed high sensitivity to the degree of sputter cleaning by a Ne-ion beam (9). Indeed, the photoemission spectra were close to those of Cr_2O_3, and only with repeated sputter cleaning was intensity near E_F obtained. The above properties suggest that this is an ideal half-metallic system in which the intergrain barrier may be systematically tuned.

Examination of the magnetotransport properties of our films reveals the signature of intergrain tunneling MR by a large drop in ρ at low magnetic fields (Fig. 4, inset). In a simplified picture of this process, neighboring grains tend to be magnetically antialigned by dipole coupling in zero applied field, and majority-spin carriers in one grain correspond to minority-spin carriers in the next (which have a gap at E_F) and thus cannot propagate. A small applied field magnetically aligns the grains, which effectively turns on a density of extended states. In the film with lower ρ, the MR ($\Delta\rho/\rho_o$) is −10% at 5 K and 2 T, whereas the annealed film is −24% at 5 K and 2 T. The approximate magnitude of the

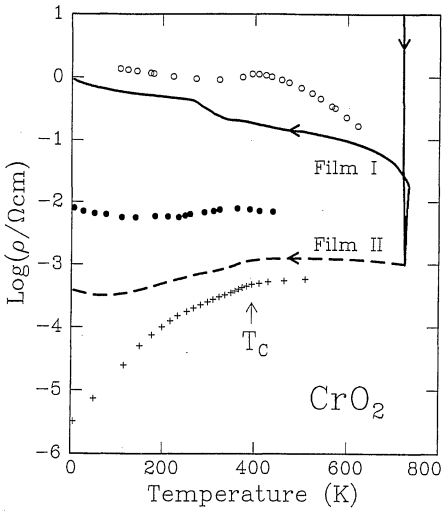

Fig. 1. The wide variation in the temperature-dependent resistivity $\rho(T)$ for samples of CrO_2. Open circles show a bulk polycrystalline sample (*12*), closed circles show another bulk polycrystalline sample (*13*), and crosses show a single-crystal film grown on TiO_2 (*14*). Two of our polycrystalline films grown on $SrTiO_3$ are also shown. Film II (dashed line) was cooled just after the formation of CrO_2 at 722 K in 200-bar O_2. Film I (solid line) was further heated to 734 K before cooling, allowing the partial decomposition of CrO_2 into Cr_2O_3, which results in significantly higher ρ.

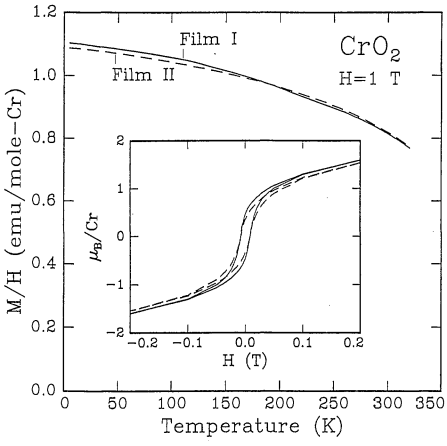

Fig. 2. The magnetic properties of the two polycrystalline films (film I, solid lines; film II, dashed lines). The temperature-dependent magnetization was taken while warming the film in 1 T. (**Inset**) Magnetization curves taken at 5 K.

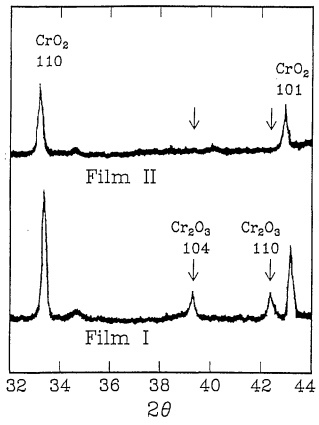

Fig. 3. A comparison of the x-ray diffraction pattern taken from the two polycrystalline films. Film II, the lower ρ film, shows only CrO_2 peaks, whereas film I, the higher ρ film, shows both CrO_2 and Cr_2O_3 peaks.

low-field MR extrapolated to $H = 0$, MR* shows roughly a factor of 3 enhancement observed for all temperatures (Fig. 4). This enhancement appears to correlate with the larger effective intergrain barrier formed by the annealing process discussed earlier. This suggests that the description of transport at the grain boundaries evolves from a field-dependent scattering process to tunneling with increasing ρ and MR.

Our study of polycrystalline films provides a new candidate for high-MR media. In recent years, there has been much interest in magnetoresistive oxides and artificial structures derived from them. Although very important for achieving and understanding new physical properties, examples requiring epitaxial multilayer growth are unlikely to be directly transferred to applications because of the high cost of preparation. By comparison, polycrystalline films of CrO_2 readily grow on a wide range of substrates, and annealing steps can greatly improve the intergrain properties by using surface-decomposed Cr_2O_3 as a tunnel barrier. Thus, the materials aspects of polycrystalline films of CrO_2 appear to be quite attractive for possible applications. The predominant issue to be resolved is the origin of the rapid decrease in MR* with increasing temperature, which is quite similar to that observed in polycrystalline perovskite manganites and thin-film trilayer tunnel junctions of perovskite manganites (*3*, *5*). Is this temperature dependence intrinsic, or can it be raised to higher temperatures by improving the materials interface properties (controlling impurity states, for example), in analogy to the successful development of magnetic metallic multilayers as useful room-temperature devices after the initial discovery of giant MR at low temperatures (*15*)? Our results demonstrate the promise of a nanocomposite materials engineering approach for designing useful MR properties, and perhaps for addressing this important question.

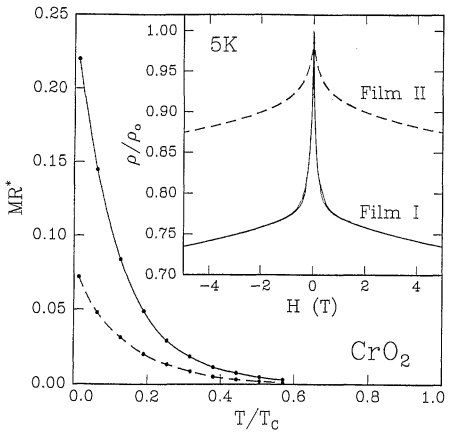

Fig. 4. The magnetoresistance (MR) of the two polycrystalline films (film I, solid lines; film II, dashed lines). (**Inset**) The field-dependent ρ at 5 K normalized to the maximum value. The main panel displays the temperature dependence of the magnitude of the low-field MR extrapolated to $H = 0$, MR*.

REFERENCES AND NOTES

1. R. A. de Groot, F. M. Mueller, P. G. van Engen, K. H. J. Buschow, *Phys. Rev. Lett.* **50**, 2024 (1983).
2. M. K. Gubkin, T. M. Perekalina, A. V. Bykov, V. A. Chubarenko, *Phys. Solid State* **35**, 728 (1993).
3. H. Y. Hwang, S.-W. Cheong, N. P. Ong, B. Batlogg, *Phys. Rev. Lett.* **77**, 2041 (1996).
4. T. Kimura *et al.*, *Science* **274**, 1698 (1996).
5. J. Z. Sun *et al.*, *Appl. Phys. Lett.* **69**, 3266 (1996).
6. H. Y. Hwang and S.-W. Cheong, unpublished results.
7. V. A. Vas'ko *et al.*, *Phys. Rev. Lett.* **78**, 1134 (1997).
8. K. Schwarz, *J. Phys. F* **16**, L211 (1986).
9. K. P. Kämper, W. Schmitt, G. Güntherodt, R. J. Gambino, R. Ruf, *Phys. Rev. Lett.* **59**, 2788 (1987).
10. R. Wiesendanger, H.-J. Güntherodt, G. Güntherodt, R. J. Gambino, R. Ruf, *ibid.* **65**, 247 (1990).
11. B. L. Chamberland, *CRC Crit. Rev. Solid State Mat. Sci.* **7**, 1 (1977).
12. B. Kubota and E. Hirota, *J. Phys. Soc. Jpn.* **16**, 345 (1960).
13. D. S. Chapin, J. A. Kafalas, J. M. Honig, *J. Phys. Chem.* **69**, 1402 (1965).
14. D. S. Rodbell, J. M. Lommel, R. C. DeVries, *J. Phys. Soc. Jpn.* **21**, 2430 (1966).
15. See, for example, P. M. Levy, *Science* **256**, 972 (1992).

16. We thank B. Barber for assistance with the SEM studies, and B. Batlogg and Y. Suzuki for helpful discussions.

2 August 1997; accepted 22 October 1997

Imaging of Intermittency in Ripple-Wave Turbulence

William B. Wright, R. Budakian, D. J. Pine,* S. J. Putterman†

The dynamics of a fluid surface filled with high-amplitude ripples were studied with a technique (diffusing light photography) that resolves the height at all locations instantaneously. Even when nonlinearities are strong enough to generate a (Kolmogorov) cascade from long wavelength (where energy is input) to shorter wavelength, the resulting turbulent state contains large coherent spatial structures. The appearance of these structures in a thermal equilibrium state (with the same average energy) would be highly improbable.

An attempt to distill into one question the issue that has intrigued scientists about the turbulent motion of fluids is, How does fully developed turbulence differ from thermal noise with the same energy? (*1*). To address this issue, we used diffusing light images of a strongly rippled surface to quantify the competition between structure formation and randomization of energy in far-off equilibrium fluid motion that must be contained in a unified theory of turbulence.

Thermal equilibrium differs from turbulence in that thermal equilibrium is global whereas the spectrum of turbulence has end points. Turbulence is driven by an external source of energy that enters at long wavelengths and then, through nonlinear interactions, cascades through an inertial region of shorter wavelengths until the energy reaches a wavelength that is so small that viscosity dominates the motion (*2*–*4*).

In the steady state, the spectrum of energy in thermal equilibrium and in the inertial range of turbulence are both power laws in the wavenumber k. For example, the equilibrium distribution of thermal energy for capillary waves per unit area of surface per range of wavenumber is

$$u(k) \approx (k_B T)k \qquad (1)$$

which expresses the equipartition of energy (k_B is Boltzmann's constant and T is temperature). In comparison the steady-state wave turbulent distribution of ripple energy driven by a source of power per unit area q is

$$u(k) \approx q^{1/2}(\rho\sigma)^{1/4}k^{-7/4} \qquad (2)$$

where ρ is the fluid density and σ is the surface tension (*5*–*7*). [For vortex turbulence as analyzed by Kolmogorov, $u(k) \sim \rho^{1/3}q^{2/3}k^{-5/3}$ where q is now the power input per unit of volume by the tides into the stirring of the seas (*3*, *4*, *8*, *9*).]

The challenges posed by turbulence are much deeper than the need to explain the different values for the exponent of k in the equilibrium (Eq. 1) and far-from-equilibrium (Eq. 2) steady states. The distinct physical aspects of turbulence are to be found in the fluctuations around the steady state. Because motion is characterized by phase as well as amplitude, the spectra (Eqs. 1 and 2) do not uniquely determine the state of fluid motion to

Physics Department, University of California, Los Angeles, CA 90095, USA.

*Present address: Department of Chemical Engineering, University of California, Santa Barbara, CA 93106, USA.
†To whom correspondence should be addressed.